DYNAMICS OF SECONDARY DROP BREAKUP—A RATE CONTROLLING PROCESS IN DENSE SPRAYS

G.M. Faeth
gmfaeth@umich.edu
Department of Aerospace Engineering
The University of Michigan
Ann Arbor, Michigan 48109-2140 U.S.A.

Abstract
Recent progress toward understanding secondary drop breakup is reviewed, considering both experimental and computational studies but limited to step changes of ambient velocities, i.e., to secondary breakup due to classical shock wave disturbances. Experimental studies of secondary breakup have concentrated on large liquid/gas density ratios because this simplifies apparatus development and measurements. Initial work along these lines established deformation and breakup regimes, and drop size and velocity distributions after breakup as jump conditions, assuming that breakup times were small compared to times required for significant changes of the spray environment. These results confirmed a proposal due to Levich (1962) that significant effects of liquid viscosity (characterized by large Ohnesorge number conditions) would inhibit secondary drop deformation and breakup compared to the secondary breakup criteria of Hinze (1955). Later measurements raised questions about the use of jump conditions to represent secondary breakup properties, finding that breakup can require significant times and distances within the dense spray region near an injector exit; therefore, subsequent experimental studies at large liquid/gas density ratios considered the temporal properties of secondary breakup. These studies found the drop size and velocity distributions of drops formed by secondary breakup, as well as rates of liquid breakup, as a function of time during the breakup process. Finally, recent numerical simulations of drop deformation and secondary breakup have been able to consider large variations of liquid/gas density ratios and Reynolds numbers that are difficult to address using experiments. These studies have shown that effects of liquid/gas density ratios and Reynolds numbers are relatively small for values greater than 8 and 50, respectively, which are typical of past experimental conditions and are representative of most practical sprays. Numerical simulations have shown that smaller values of these parameters, however, significantly inhibit drop deformation and secondary breakup.

Introduction

The secondary breakup of drops is an important multiphase flow process with applications to liquid atomization, dispersed multiphase flow, combustion instability of sprays, heterogeneous detonations of liquid/gas mixtures, the properties of rain, and interactions between high-speed vehicles and raindrops, among others. In particular, recent studies have confirmed the conventional view of liquid atomization that drops formed by primary breakup at liquid surfaces are intrinsically unstable to secondary breakup. In addition, secondary breakup is often the rate-controlling process within dense sprays in much the same way that drop vaporization is often the rate-controlling process within dilute sprays. Motivated by these observations, recent findings concerning secondary drop breakup are reviewed in this paper, considering results obtained from both experimental and computational studies.

There have been numerous studies of both noncombusting and combusting sprays, mainly emphasizing the dilute spray region far from the injector exit, where observations and modeling are relatively tractable because liquid volume fractions are relatively small. As a result, many features of dilute sprays are understood reasonably well, see reviews due to Giffen and Muraszew [1], Levich [2], Clift et al. [3], Lefebvre [4], Wierzba and Takayama [5], Faeth and coworkers [6-9], and references cited therein. Thus, attention is now being directed to the less accessible dense-spray region near the injector exit, in order to determine how injector design properties and the spray environment influence the drop-containing dispersed flow entering the dilute-spray region. Ruff et al. [10-12], Tseng et al. [13,14] and Sallam and coworkers [15-17] have undertaken a series of studies of the dense spray region near the injector exit for the classical configuration of nonevaporating round nonturbulent and turbulent liquid jets in still gaseous environments. They found that this region consisted of an all liquid core that typically extended on the order

of 100 injector diameters from the jet exit with drops forming along the surface of the liquid core due to primary breakup as well as from breakup of the liquid core itself at its downstream end. It was also found that the large liquid volume fractions observed in dense sprays generally were due to the presence of the liquid core; in contrast, liquid volume fractions in the dispersed flow region surrounding the liquid core generally were small, less than 0.1%, so that the dense spray region actually corresponds to a dilute spray but with added complications due to the presence of the liquid core and irregular liquid ligaments and drops (Note that Sallam and Faeth [17] recently found that larger liquid volume fractions, 1-10%, are present in the dispersed flow region just after the location where the liquid core itself breaks up). These observations also supported the traditional view of atomization, expressed by Giffen and Muraszew [1], that primary breakup at the surface of the liquid core is followed by secondary breakup in a dilute spray environment where effects of drop collisions are small (except for sprays that seek breakup by collisions such as impinging injectors). Finally, rates of mixing, drop properties and flow structure within dense sprays are strongly dependent on the degree of flow development and turbulence levels at the jet exit, and on the liquid/gas density ratio, somewhat analogous to the effect of these properties on the structure of the flow development region of single-phase jets.

To summarize, recent work has demonstrated that secondary breakup is an important process of dense sprays because primary breakup at the surface of the liquid core yields drops that are intrinsically unstable to secondary breakup. In addition, the distances and times required to complete secondary breakup are not small compared to the dimensions and characteristic residence times of dense sprays so that secondary breakup generally must be treated as a rate process rather than by jump conditions, i.e., drop size and velocity distributions and rates of drop formation due to secondary breakup must be known as a function of time during breakup. Finally, high-pressure spray combustion processes for typical power and propulsion systems involve conditions where viscous effects dominate surface tension effects because the surface tension becomes small as the thermodynamic critical point is approached at the liquid surface; for the same reasons, liquid/gas density ratios approach unity at this condition. As a result, effects of wide variations of surface tension and liquid/gas density ratio on secondary breakup properties must be known in order to address practical applications. These issues will be addressed in the following, considering studies emphasizing experimental and computational methods, in turn.

Measurements of Secondary Breakup

Introduction. Giffen and Muraszew [1],], Levich [2], Clift et al. [3], Lefebvre [4], Wierzba and Takayama [5], Faeth [6,7], Hinze [18] and Krzeczkowski [19] have reviewed early studies of secondary breakup; therefore, the following discussion will emphasize more recent studies. Of particular interest are the experimental studies of Hsiang and Faeth [20-22] who considered secondary breakup regimes and outcomes as jump conditions (assuming small breakup times and distances) and Chou et al. [23,24] and Dai and Faeth [25] who considered the dynamics of secondary breakup by resolving breakup outcomes as a function of time during the breakup process. These studies involved exposing freely falling drops to shock wave disturbances propagating in the horizontal direction within a shock tube; pulsed holography and shadowgraphy were used to observe the breakup process, exploiting the capabilities of holography to freeze the entire flow field for later detailed analysis (much like post-processing a complete numerical simulation of breakup but replacing the simulation by an actual experiment). Experimental results seeking jump conditions and time resolved breakup properties will be considered, in turn, in the following.

Deformation and Breakup Regimes. Numerous studies have considered the definitions and conditions for the onset of various deformation and breakup regimes of drops subjected to shock wave disturbances when effects of liquid viscosity are small. The breakup regime observed at the onset of breakup is called bag breakup; it involves deflection of the drop into a thin disk positioned normal to the flow direction, followed by deformation of the center of the disk into a thin balloon-like structure (with the open end facing upstream), both of which subsequently divide into drops (see Wierzba and Takayama [5], Hinze [18] and Krzeczkowski [19], Chou et al. [23,24], Dai and Faeth [25], Hansen et al. [26], Gel'fand [27], Ranger and Nicholls [28], and Reineke and coworkers [29,30] for photographs of secondary breakup in all the breakup regimes discussed here). The shear breakup regime is observed at larger relative velocities than bag breakup; it involves deflection of the periphery of the disk in the downstream direction, rather than the center, and the stripping of drops from the periphery of the disk. The transition between the bag and shear breakup regimes is a complex mixture of the two bounding regimes that will be denoted the multimode regime in the following (see Dai and Faeth [25] for photographs of the several breakup behaviors observed in the multimode regime). Finally, a complex breakup mechanism has been observed at very large relative velocities that has been called catastrophic breakup by Reineke and coworkers [29,30]; nevertheless, this regime is not seen in

typical dense sprays (but it is important for pulsed detonation liquid propulsion systems) and will not be considered here.

Existing experimental observations of secondary breakup have generally involved liquid/gas density ratios greater than 500 and drop Reynolds numbers greater than 50. At these conditions, Hinze [18] developed a very convenient way to correlate breakup regime transitions as a breakup regime map plotted in terms of the Weber, We, and Ohnesorge, Oh, numbers, which are measures of the ratios of drag and liquid-viscous forces to surface-tension forces, respectively. The motivation for this plot can be seen by noting that gas dynamic forces, proportional to $\rho_g u^2$, can only be stabilized by surface-tension forces, σ/d, when liquid-viscous forces are small, whereas gas dynamic forces can only be stabilized by liquid-viscous forces, $\mu_f u_f/d = \mu_f(\rho_g/\rho_f)^{1/2} u/d$, when surface tension forces are small (adopting the expression of Ranger and Nicholls [28] to relate gas and liquid velocities). Thus,

$$\sigma/d \sim \rho_g u^2, \ \mu_f \text{ small}; \quad \mu_f(\rho_g/\rho_f)^{1/2} u/d \sim \rho_g u^2, \quad \sigma \text{ small} \tag{1}$$

which implies that breakup transitions when liquid-viscous forces and surface-tension forces are small, take on the following forms, respectively:

$$We_{cr} = \text{const.}, \quad Oh << 1; \qquad We_{cr} \sim Oh^2, \quad Oh >> 1 \tag{2}$$

It has also been found that the maximum deformation properties of drops subjected to shock wave disturbances can be correlated in terms of the same variables, which is not surprising due to the close relationship between deformation and breakup.

The resulting deformation and breakup regime map based on the ideas of Hinze [18] appears in Fig. 1. Measurements illustrated in this figure were drawn from Hansen [26], Hinze [18], Lane [31], Loparev [32] and Hsiang and Faeth [20,22], whereas correlations of the deformation and breakup regime boundaries were obtained from Krzeczkowski [19] and Hsiang and Faeth [22] which are in excellent agreement with each other. The results illustrated in Fig. 1 support the results of Eqs. (2); namely, that the values of We at the transitions are relatively independent of Oh when Oh << 1 whereas $We_{cr} \sim Oh^2$ when Oh >> 1. At small Oh, the various breakup regimes that were just discussed—bag, multimode, and shear breakup—can all be seen along with an oscillatory deformation regime that is defined by conditions where the drop oscillates with a weakly-damped amplitude, see Hsiang and Faeth [20] for a discussion of this behavior. Increased damping due to increased effects of liquid viscosity cause the oscillatory regime to disappear as Oh increases. Notably, large Oh also suppresses the bag and (probably) to the multimode regimes, eventually leaving only the shear breakup mechanism. Aalburg et al. [33] report other findings at large Oh conditions based on numerical simulation of drop deformation in response to shock wave disturbances; these results will be discussed later.

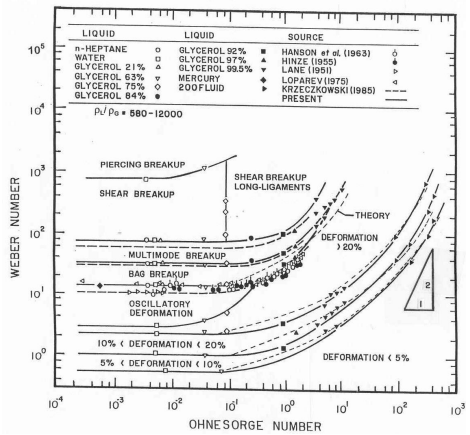

Figure 1. Drop deformation and secondary breakup regime map for shock wave disturbances.

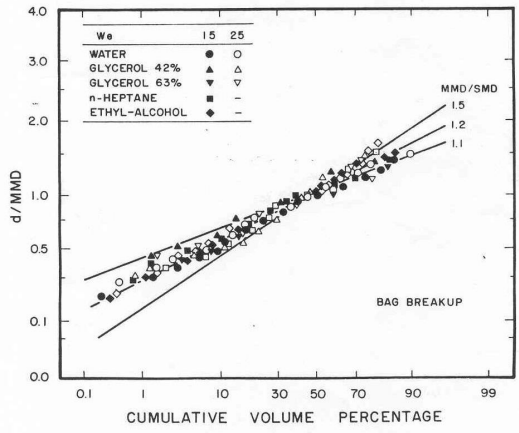

Figure 2. Distribution of drop diameters after shear breakup.

Breakup Outcomes. Assuming that breakup times and distances are small compared to characteristic dense spray residence times and distances, secondary breakup can be treated using jump conditions that provide drop size

and velocity distributions after breakup. Gel'fand et al. [34] provided information of this type for bag breakup but this information is too limited for adequate treatment of the properties of drops formed by secondary breakup. Later work by Hsiang and Faeth [20-22] using pulsed holography achieved a more complete description of the outcomes of secondary breakup for shock wave disturbances at liquid/gas density ratios greater than 500 and Oh < 0.1. Some of the main findings of this work will be discussed in the following.

Ruff et al. [12] and Tseng et al. [14] found that drop size distributions at each point in dense sprays were well correlated by Simmons' [35] universal root normal distribution with MMD/SMD = 1.2, see Belz [36] for the properties of this function. Remarkably, drop size distributions after secondary breakup also generally satisfy the same distribution (but only if the core or drop forming drop is removed from the distribution for shear breakup). This correlation is illustrated in Fig. 2 for bag breakup involving a variety of drop liquids and Weber numbers for liquid/gas density ratios greater than 500 and Ohnesorge numbers smaller than 0.1. The root normal distribution function is a two parameter correlation and with MMD/SMD specified is only a function of the SMD. Thus, given the universal root normal drop size distribution function, drop sizes are fully specified by the SMD alone, providing a very compact way of describing the outcome of secondary breakup (except for shear breakup where the properties of the core drop must be described independently as well).

A correlating expression for the SMD after secondary breakup was developed considering the shear breakup regime [20]. It was assumed that liquid was stripped from the periphery of the core drop to form drops by secondary breakup. Other assumptions of this simplified (phenomenological) analysis are as follows: the relative velocity at the time of breakup was taken to be equal to the initial relative velocity, the diameters of drops formed by secondary breakup were taken to be comparable to the thickness of the laminar boundary layer that forms in the liquid along the front surface of the drop due to its motion, the characteristic liquid phase velocities were found as suggested by Ranger and Nicholls [28] similar to the approach used in Eqs. (1) and (2), and the SMD is dominated by the largest drop sizes in the distribution so that the length of the liquid phase boundary layer is proportional to d_o. Based on these ideas, the following expression was obtained as the best fit of available SMD measurements after secondary drop breakup, see Hsiang and Faeth [20]:

$$\rho_g \, SMD \, u_o^2/\sigma = 6.2(\rho_f/\rho_g)^{1/2}(\mu_f/(\rho_f d_o u_o))^{1/2}We \tag{3}$$

Surface tension has been introduced into Eq. (3) in order to highlight the potential secondary breakup properties of drops formed by shear breakup. Consistent with the derivation of Eq. (3), however, surface tension does not influence the final SMD, e.g., Eq. (3) can be simplified as follows:

$$SMD/d_o = 6.2/Re_f^{1/2} \tag{4}$$

The form of Eq. (4) is analogous to the expression for the thickness of a laminar boundary layer along a surface of length d_o in a liquid, highlighting the relationship between the thickness of this layer and drop sizes produced by shear breakup.

Available measurements of SMD after breakup, along with the correlation of Eq. (3), are illustrated in Fig. 3. Remarkably, a single correlation developed for shear breakup expresses the SMD after breakup in all regimes. This behavior still needs to be explained although other properties like the breakup time are also relatively independent of the breakup regime, see Hsiang and Faeth [20] and Dai and Faeth [25]. The results illustrated in Fig. 3 are in terms of a Weber number based on the SMD after breakup and the initial relative velocity. Superficially, it is evident that this Weber number exceeds critical Weber numbers for secondary breakup at small Oh, as indicated on the plot; this implies that a large fraction of the drops formed by breakup should still be unstable for subsequent breakup. Nevertheless, there was no evidence of subsequent breakup of large drops. This stability was particularly illustrated by the core or drop-forming drop during shear breakup, which is the largest drop after secondary breakup is completed. Studying these core drops, it was found that three requirements must be satisfied for secondary breakup to occur, as follows: sufficient time after the velocity disturbance is imposed is needed to achieve degrees of drop deformation required for drop formation by secondary breakup, e.g., $t_{cr}/t^* > 2$; the flow disturbance must be sufficiently strong to form drops by secondary breakup, e.g., $We_{cr} > 13$; and the local rate of acceleration of the drop must be sufficiently large, e.g., $Eo_{cr} = a\rho_f d^2/\sigma > 16$, see Hsiang and Faeth [21]. This information can be combined with a correlation for the core drop velocity, as discussed by Hsiang and Faeth [21], to provide the diameter and velocity of the core drop after breakup, while properly allowing for the three breakup requirements that were just noted.

With information available for drop diameter distributions and core drop diameters and velocities, after secondary breakup, the final problem involves finding the correlation between drop diameters and velocities (except for the core drop) after breakup. Simplified phenomenological analysis, and fitting with available measurements, yields the following expression [21]:

$$u_o/u_b = 1 + 2.7((\rho_g/\rho_f)^{1/2} d_o/d)^{2/3} \quad (5)$$

where u_b is the velocity of a drop having a diameter d after secondary breakup has ended. This expression properly allows for the fact that small drops formed early in the breakup process more closely approach the ambient gas velocity than large drops formed late in the breakup process.

Finally, the variation of drop velocities and the time of drop formation with drop size implies that secondary breakup extends over a considerable region of space. For example, core drops move 30-40 initial drop diameters during breakup whereas the largest and smallest drops after breakup become separated by more than 100 initial drop diameters. Thus, secondary breakup is more properly treated as a rate process, rather than by jump conditions, in some instances.

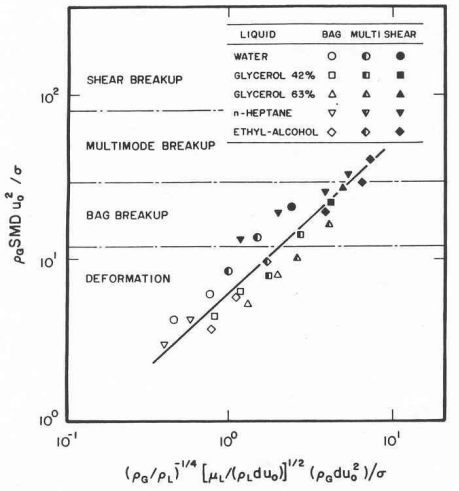

Figure 3. Correlation of the SMD after secondary breakup.

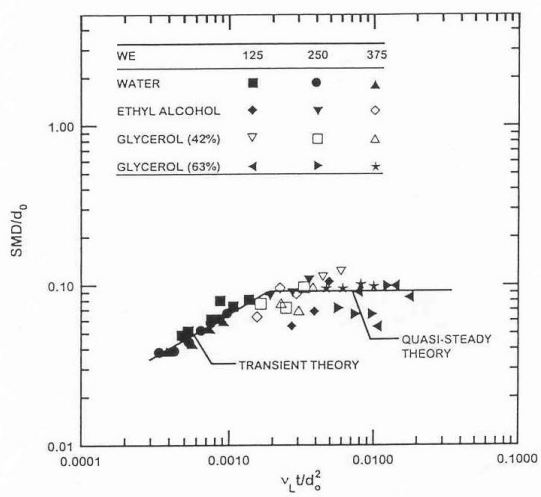

Figure 4. Temporal variation of the SMD of drops produced by shear breakup.

Breakup Dynamics. Measurements of the dynamics of secondary drop breakup have been undertaken by Chou et al. [23] for shear breakup, by Chou et al. [24] for bag breakup, and by Dai and Faeth [25] for multimode breakup. These experiments involve the same experimental techniques as Hsiang and Faeth [20-22] and similarly were limited to liquid/gas density ratios greater than 500 and drop Reynolds numbers greater than 50.

For shear breakup, Chou et al. [23] find that the size distributions of drops formed by secondary drop breakup satisfy Simmons' [35] universal root normal distribution function with MMD/SMD = 1.2 at each instant of time whereas the velocity distributions of drops formed by secondary breakup are uniform (independent of drop size) at each instant of time. For bag breakup, however, Chou et al. [24] find a different dynamic behavior: drops formed from the bag are nearly monodisperse and have mean diameters of roughly 4% of the initial drop diameter, drops formed from the basal ring at the base of the bag are nearly monodisperse and have mean diameters of roughly 30% of the initial drop diameter, and each of these drop populations have velocity distributions that are nearly uniform (although the two populations have different velocities). Finally, Dai and Faeth [25] find more complex behavior of size and velocity distributions of drops formed by secondary breakup in the multimode regime as it evolves from near-bag to near-shear breakup behavior.

The dynamic aspects of shear breakup are qualitatively similar to outcomes of the entire shear breakup process and were addressed similar to the shear breakup jump conditions. Two types of behavior could be identified for drop formation by shear breakup, as follows: (1) an initial transient phase where the thickness of the boundary layer in the liquid drop, and thus the sizes of drops formed from it, increases as a function of time similar to the transient growth of boundary layers along surfaces; and (2) a quasi-steady period where the thickness of the boundary layer in the liquid drop becomes a fixed fraction of the drop diameter. Based on phenomenological analysis of these two

regimes, the following expressions for the SMD as a function of time were obtained by best fitting the measurements:

$$SMD/d_o = 2.0(\nu_f t/d_o^2)^{1/2}, \quad t < t_c; \qquad SMD/d_o = 0.09, \quad t > t_c \tag{6}$$

where $\nu_f t_c/d_o^2 = 0.002$. Naturally, this breakup process only continues until the breakup time for shear breakup, $t_b/t^* = 6.0$ is reached, see Dai and Faeth [25]. The measurements of SMD as a function of time for shear breakup due to Chou et al. [23] are illustrated in Fig. 4 considering various liquids and three Weber numbers in the shear breakup regime. The correlations of Eq. (6) are quite good in the transient regime but exhibit somewhat greater scatter in the quasi-steady regime.

The velocities of drops formed by shear breakup were uniform at each instant of time and streamwise velocities were related to the streamwise velocity of the core (or drop-forming) drop at the same time, as follows [23]:

$$(u-u_c)/(u_o-u_c) = 0.37 \tag{7}$$

whereas the mean cross-stream velocity was essentially zero. This result suggests appreciable acceleration of the drop liquid during breakup, mainly as a result of the momentum of the liquid in the boundary layer near the drop surface and in the ligaments formed by this layer before it breaks up into drops. An expression for the streamwise velocity of the core drop as a function of time can be obtained from Hsiang and Faeth [21], as follows:

$$u_o/u_c = 1 + 3.75(t/t^*)(\rho_g/\rho_f)^{1/2} \tag{8}$$

The final property needed to define the temporal properties of shear breakup for large liquid/gas density ratios involves the mass rate of formation of dispersed drops due to shear breakup. Chou et al. [23] found that the mass rate of formation of dispersed drops for shear breakup could be represented by a clipped-Gaussian function with liquid removal from the parent drop beginning and ending at $t/t^* = 1.5$ and 5.5, respectively.

Chou et al. [24] and Dai and Faeth [25] report similar results, e.g., drop size and velocity distributions, and mass rates of formation of dispersed drops, as a function of time within the bag and multimode breakup regimes in much the same manner as presented here for the shear breakup regime; these sources should be considered for the details of these results.

Conclusions. Secondary breakup of drops, emphasizing liquid/gas density ratios greater than 500, Reynolds numbers greater than 50, and shock wave disturbances, have been studied experimentally. The objectives have been to better understand breakup regimes, drop properties after breakup as jump conditions for conditions where breakup times and distances are small compared to characteristic breakup times and distances of the spray, and the temporal variation of drop properties after breakup, as well as the rate of dispersed drop formation by breakup, as a function of time during breakup for conditions where breakup cannot be treated using jump conditions. The major conclusions of these considerations are as follows:

1. Drop deformation and breakup begin at $We_{cr} \sim 1$, and 10 for $Oh < 0.1$, however, $We_{cr} \sim Oh^2$ for $Oh > 10$ because the mechanism of drop stabilization shifts from surface tension dominated to liquid viscosity dominated as the Oh increases.
2. Information about the outcome of secondary drop breakup, as jump conditions, has been developed for conditions where effects of liquid viscosity on deformation and breakup regime boundaries are small ($Oh < 0.1$). These results provide correlations of drop size and velocity distributions after breakup based on simplified phenomenological analyses. An interesting feature of these results is that whereas deformation and breakup transitions depend on surface tension and not liquid viscosity, drop sizes after breakup depend on liquid viscosity and not surface tension, somewhat analogous to the way that fluid viscosity affects transition to turbulence but has little effect of turbulent mixing thereafter.
3. Information about the temporal variation of the outcome of secondary drop breakup has been developed for conditions where effects of liquid viscosity on deformation and breakup regime boundaries are small ($Oh < 0.1$). These results provide correlations of drop size and velocity distributions after breakup, and rates of formation of dispersed drop liquid, as a function of time during breakup based on simplified phenomenological analyses.

Aside from the deformation and breakup regime map, existing information about secondary breakup (e.g., drop size and velocity distributions after breakup and drop size and velocity distributions and rates of liquid breakup as a function of time during breakup) is limited to Oh < 0.1, liquid/gas density ratios greater than 500, Reynolds numbers greater than 50 and shock wave disturbances. Clearly, effects of Oh, liquid/gas density ratios, Reynolds numbers and type of disturbance merit additional study in order to better understand the secondary breakup properties of practical sprays. Results along these lines based on computations of drop deformation due to shock wave disturbances will be considered next.

Computations of Drop Deformation

Introduction. Past studies of Hsiang and Faeth [20-22], Chou et al. [23,24] and Dai and Faeth [25] have involved measurements of the outcomes of secondary breakup of drops subjected to shock wave disturbances. This work has provided information about the properties of drops produced by breakup at the end of the breakup process (or jump conditions) as well as the temporal variation of the properties of drops produced during the breakup process. Due to experimental constraints, however, these results were limited to liquid/gas density ratios greater than 500, Oh < 0.1 (except for the determination of deformation and breakup regime boundaries), and Reynolds numbers greater than 50. Thus, the objective of computations of drop deformation was to consider the response of drops to shock wave disturbances at the small liquid/gas density ratio, large Ohnesorge number and small Reynolds number conditions that are difficult to address by experiments but are more representative of conditions in sprays at the pressures typical of practical power and propulsion systems.

Drop breakup is a complex three-dimensional process, due to the formation of nodes and the wide range of length scales resulting from drop formation. Thus, a detailed simulation of breakup would require a three-dimensional time-dependent computation with a locally very fine numerical grid that is not tractable for practical numerical computations using available computer facilities. Experimental results of Hsiang and Faeth [20-23], however, show that the onset of drop breakup conditions can be associated with specific degrees of drop deformation. Adopting this finding, it was possible to estimate conditions at the onset of breakup using simplified computations of drop deformation alone.

The results of numerical simulations of drop deformation (and drop breakup properties based on inference from drop deformation properties as just discussed) due to Aalburg et al. [33] will be discussed next, considering effects of Weber number, Ohnesorge number, Reynolds number, liquid/gas density ratio and liquid/gas viscosity ratio on drop deformation (and by inference, on secondary drop breakup).

Computational Methods. Numerical simulations of drop deformation involved solving the time-dependent, incompressible and axisymmetric Navier-Stokes equations using the projection method of Chorin [37] in conjunction with the marker and cell (MAC) method of Harlow and Welch [38]. The level set method of Sussman et al. [39] was used to capture the liquid/gas interface, using the redistancing algorithm of Sussman and Fatemi [40] to maintain the level set as an accurate distance function. The surface interface conditions were treated following Brackbill et al. [41]. Finally, buoyancy was neglected and the flow was assumed to be isothermal with constant liquid and gas phase properties and negligible evaporation.

Evaluation of Computations. The numerical simulations were evaluated by comparison of predictions and measurements, as follows: predicted wake lengths behind non-deforming spherical drops as a function of Reynolds number for values smaller than the onset of instabilities (Re < 130) compared with the measurements of Taneda [42], predicted drag coefficients of nondeforming spherical drops as a function of Reynolds number (Re < 1000) compared with the measurements of Roos and Willmarth [43], and predicted maximum drop deformation as a function of Weber number (2 < We < 13) compared with the measurements of Hsiang and Faeth [22]. In all cases, the agreement between predictions and measurements was well within computational accuracy and experimental (95% confidence) uncertainties.

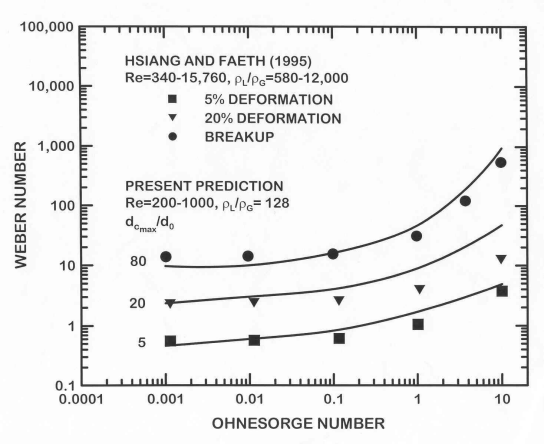

Figure 5. Measured and predicted maximum drop deformation and breakup properties.

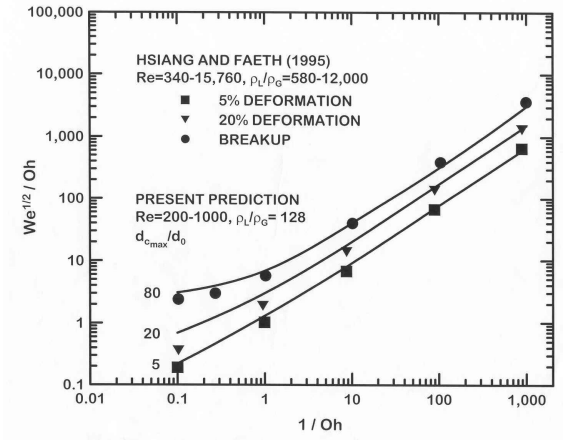

Figure 6. Drop deformation and secondary breakup regime map for shock wave disturbances.

Deformation and Breakup Regimes. Computations of drop deformation properties indicated that effects of liquid/gas density ratio were small for values greater than 8, and that effects of Reynolds number were small for values greater than 50. Thus, predictions for ρ_f/ρ_g = 128 and Re = 200-1000 were evaluated by comparison with the measurements of Hsiang and Faeth [23] that were carried out at values of ρ_f/ρ_g and Re larger than the limits just mentioned. The results are illustrated in Fig. 5 which is plotted according to the Hinze [18] deformation and breakup regime map illustrated in Fig. 1. It is evident that the numerical simulations are in reasonably good agreement with the measurements, that both predictions and measurements indicate increased resistance to deformation (and breakup) as Oh increases as indicated in connection with Fig. 1, and that a maximum deformation of 80% provides a very good correlation of conditions where secondary drop breakup occurs. On the other hand, the numerical simulations revealed an undesirable effect of liquid/gas viscosity ratio, μ_f/μ_g, on deformation and breakup properties at large Oh that was not recognized before; namely, that onset conditions at large Oh involve a rather restrictive range of μ_f/μ_g on this type of plot, that is not typical of all practical applications (although this ratio was similar for both predictions and measurements in Fig. 5), see Aalburg et al. [33] for more details about this behavior.

The large effect of μ_f/μ_g on the Hinze [18] form of the deformation and breakup regime map is not desirable and an alternative was sought. A better approach for representing conditions where effects of liquid viscosity are large (large Oh) was found by accounting for viscous effects directly by plotting the ratio of drag/liquid-viscous forces, $We^{1/2}/Oh$, instead of the ratio of drag to surface tension forces, We (note that the new parameter intrinsically agrees with the relationship $We \sim Oh^2$ at the breakup boundary discussed in connection with Fig. 1). Figure 6 is an illustration of the deformation and breakup regime map in the new coordinates, plotting deformation and breakup regime boundaries as a function of $We^{1/2}/Oh$ and 1/Oh (the last chosen so that the general shape of the map is unchanged). In this form, the predictions and measurements of deformation continue to be in good agreement, the 80% deformation condition is still a good representation of breakup conditions but effects of variations of μ_f/μ_g now only impact properties at small values of 1/Oh where the deformation and breakup lines are nearly horizontal and the change of μ_f/μ_g has essentially no effect. Thus, the approach illustrated in Fig. 6 yields secondary drop deformation and breakup regime boundaries that are relatively independent of ρ_f/ρ_g for values greater than 8, and Re for values greater than 50, and are in excellent agreement with existing measurements of the deformation and breakup properties at the same limiting conditions.

The numerical predictions provided information about other aspects of drop deformation and breakup in response to shock wave disturbances that have not been revealed by experiments. First of all, predictions of particular deformation and breakup regime boundaries exhibited negligible effects of ρ_f/ρ_g variations in the range 8-∞ when Oh < 0.1. This effect, combined with the small effect of Re for values greater than 50 and the fact that most past measurements of deformation and breakup regime boundaries were carried out for Oh < 0.1, no doubt accounts for the robustness of the Hinze [18] treatment of these boundaries. On the other hand, the values of We required for particular deformation and breakup conditions increase significantly as ρ_f/ρ_g decreases toward unity for ρ_f/ρ_g in the range 1-8, (particularly for large Oh conditions) and as Re decreases below 50 and approaches the Stokes range of drag behavior or spheres where the drag coefficient increases significantly (eventually becoming proportional to

1/Re). In both cases, increased resistance to drop deformation and breakup can be attributed to increased response of the drop to the drag of the gas flow. This causes relative velocities between the drop and the gas to decrease rapidly, reducing the drag stress on the drop before significant deformation (including levels needed for breakup) can occur. See Aalburg et al. [33] for other findings of the drop deformation computations.

Conclusions. Study of the deformation and breakup properties of drops subjected to shock wave disturbances, based on time-dependent numerical simulations of the process, have yielded the following major conclusions:

1. Predictions and measurements of wake and drag properties of nondeforming spheres, and the deformation and breakup properties of drops, are in good agreement for the range of conditions where they can be compared (Re < 1000 for nondeforming spheres, and $\rho_f/\rho_g > 8$ and Re > 50 for drops).
2. The liquid/gas density ratio has only a small effect on the deformation and breakup properties of drops for ρ_f/ρ_g in the range 8-∞, and Oh < 0.1, however, the resistance of drops to deformation and breakup progressively increases as the density ratio approaches unity in the range 1-8, particularly at large Oh conditions.
3. The effects of Re are small for Re > 50 because the drag coefficient is relatively constant in this region, however, reduction of Re toward the Stokes range significantly increases the resistance of a drop to deformation and breakup due to the increase of drag coefficients with decreasing Reynolds number at these conditions.
4. At large Oh, surface tension has a negligible influence on drop deformation and breakup and the conventional Hinze [18] deformation and breakup regime map exhibits some undesirable effects of liquid/gas density and viscosity ratios. This problem can be avoided by plotting the map in terms of the ratio of drag/liquid-viscous forces, $We^{1/2}/Oh$, as a function of the ratio of surface-tension/liquid-viscous forces, 1/Oh; the alternative approach reduces effects of parameters such as ρ_f/ρ_g and Re for values greater than 8 and 50, respectively. For smaller values of these parameters, the effects mentioned in connection with conclusions 2 and 3 become important and must be considered for accurate estimates of drop deformation and breakup properties.

Numerical simulations considered thus far still have not adequately quantified effects of small ρ_f/ρ_g and Re. In particular, deformation properties should be predicted reasonably well for these conditions so the computed results would be helpful. Naturally, new experiments for the same range of conditions would also be very useful for evaluating the predictions.

Other objectives noted at the end of the section on measurements of secondary breakup provide obvious objectives for numerical simulations as well. In particular, large Oh and small ρ_f/ρ_g conditions yield large degrees of deformation without the formation of small drops, see Hsiang and Faeth [20-22]; this behavior promotes the computational tractability of the numerical simulations that should be exploited because such conditions are very difficult to address using experiments.

Nomenclature

Symbols: a = accleration, d = drop diameter, d_{cmax} = maximum cross stream drop diameter, Eo = Eötvös number = $a\rho_f d^2/\sigma$, MMD = mass median drop diameter, Oh = Ohnesorge number = $\mu_f/(\rho_f\sigma d_o)^{1/2}$, Re = Reynolds number = $u_o d/\nu_g$, Re_f = Reynolds number of liquid = $u_f d/\nu_f$, SMD = Sauter mean diameter, t = time, t_c = shear breakup time = $0.002\ d_o^2/\nu_f$, t* = characteristic drop time = $(\rho_f/\rho_g)^{1/2} d_o/u_o$, u = drop velocity, u_b = drop velocity at end of breakup, u_c = velocity of core drop, u_f = characteristic liquid velocity, We = Weber number = $\rho_g d_o u_o^2/\sigma$; Greek Symbols: μ = molecular viscosity, ν = kinematic viscosity, ρ = density, σ = surface tension; Subscripts: b = end of breakup condition, cr = onset of breakup regime condition, f = liquid property, G = g = gas property, L = liquid property, o = initial condition.

Acknowledgments

The research described here was sponsored by the U.S. Air Force Office of Scientific Research, Grant Nos. F49620-95-1-0364, F49620-99-1-0083 and F49620-02-1-0074 under the technical management of J.M. Tishkoff. The U.S. Government is authorized to reproduce and distribute copies of this article for governmental purposes notwithstanding any copyright notation thereon.

References

[1] Giffen, E., and Muraszew, A., *The Atomization of Liquid Fuels*, Chapman & Hall, 1953.
[2] Levich, G., *Physicochemical Hydrodynamics*, Prentice-Hall, Inc., 1963, p. 639.
[3] Clift, R., Grace, J.R., and Weber, M.E., *Bubbles, Drops and Particles*, Academic Press, 1978, pp. 26 and 339.
[4] Lefebvre, A..H., *Atomization and Sprays*, Hemisphere Publishing Co., 1989.

[5] Wierzba, A., and Takayama, K., "Experimental investigation of the aerodynamic breakup of liquid drops", *AIAA J*. 26, 1329-1335 (1988).
[6] Faeth, G.M., "Mixing, transport and combustion in sprays", *Prog. Energy Combust. Sci*. 13, 293-345 (1987).
[7] Faeth, G.M., "Structure and atomization properties of dense turbulent sprays", *Proc.Combust. Inst*. 23, 1345-1352 (1990).
[8] Faeth, G.M. Hsiang, L.-P., and Wu, P.-K., "Structure and breakup properties of sprays", *Int. J. Multiphase Flow* 21 (Suppl.), 99-127 (1995).
[9] Faeth, G.M., "Spray combustion phenomena", *Proc.Combust. Inst*. 26, 1593-1612 (1996).
[10] Ruff, G.A., Sagar, A.D., and Faeth, G.M., "Structure and mixing properties of pressure-atomized sprays", *AIAA J*. 27, 901-908 (1989).
[11] Ruff, G.A., Bernal, L.P., and Faeth, G.M., "Structure of the near-injector region of non-evaporating pressure-atomized sprays", *J. Prop. Power* 7, 221-230 (1990).
[12] Ruff, G.A., Wu, P.-K., Bernal, L.P., and Faeth, G.M., "Continuous- and dispersed-phase structure of dense non-evaporating pressure-atomized sprays", *J. Prop. Power* 8, 280-289 (1992).
[13] Tseng, L.-K., Ruff, G.A., and Faeth, G.M., "Effects of gas density on the structure of liquid jets in still gases", *AIAA J*. 30, 1537-1544 (1992).
[14] Tseng, L.-K., Wu, P.-K., and Faeth, G.M., "Dispersed-phase structure of pressure-atomized sprays at various gas densities", *J. Prop. Power* 8, 1157-1166 (1992).
[15] Sallam, K.A., Dai, Z., and Faeth, G.M., "Drop formation at the surface of plane turbulent liquid jets in still gases", *Int. J. Multiphase Flow* 25, 1161-1180 (1999).
[16] Sallam, K.A., Dai, Z., and Faeth, G.M., "Liquid breakup at the surface of turbulent round liquid jets in still gases", *Int. J. Multiphase Flow* 28, 427-449 (2002).
[17] Sallam, K.A., and Faeth, G.M. (2002) "Surface properties during primary breakup of turbulent liquid jets in still air", *AIAA J*., submitted.
[18] Hinze, J.O., "Fundamentals of the hydrodynamic mechanism of splitting in dispersion processes", *AIChE J*. 1, 289-295 (1955).
[19] Krzeczkowski, S.A., "Measurement of liquid droplet disintegration mechanisms", *Int. J. Multiphase Flow* 6, 227-239 (1980).
[20] Hsiang, L.-P., and Faeth, G.M., "Near-limit drop deformation and secondary breakup", *Int. J. Multiphase Flow* 18, 635-652 (1992).
[21] Hsiang, L.-P., and Faeth, G.M., "Drop properties after secondary breakup", *Int. J. Multiphase Flow* 19, 721-735 (1993).
[22] Hsiang, L.-P., and Faeth, G.M., "Drop deformation and breakup due to shock wave and steady disturbances", *Int. J. Multiphase Flow* 21, 545-560 (1995).
[23] Chou, W.-H., Hsiang, L.-P., and Faeth, G.M., "Temporal properties of secondary drop breakup in the shear breakup regime", *Int. J. Multiphase Flow* 23, 651-669 (1997).
[24] Chou, W.-H., and Faeth, G.M., "Temporal properties of secondary drop breakup in the bag breakup regime", *Int. J. Multiphase Flow* 24, 889-912 (1998).
[25] Dai, Z., and Faeth, G.M., "Temporal properties of secondary breakup in the multimode breakup regime", *Int. J. Multiphase Flow* 27, 217-236 (2001).
[26] Hanson, A.R., Domich, E.G., and Adams, H.S., "Shock-tube investigation of the breakup of drops by air blasts", *Phys. Fluids* 6, 1070-1080 (1963).
[27] Gel'fand, B.E,, "Droplet breakup phenomena in flows with velocity lag", *Prog. Energy Combust. Sci*. 22, 201-265 (1996).
[28] Ranger, A.A., and Nicholls, J.A., "The aerodynamic shattering of liquid drops", *AIAA J*. 7, 285-290 (1969).
[29] Reinecke, W.G., and McKay, W.L., "Experiments on waterdrop breakup behind Mach 3 to 12 shocks", Sandia Corp. Report No. SC-CR-70-6063 (1969).
[30] Reinecke, W.G., and Waldman, G.D., "A study of drop breakup behind strong shocks with applications to flight", Avco Report No. AVSD-0110-70-77 (1970).
[31] Lane, W. R., "Shatter of drops in streams of air", *Ind. Engr. Chem*. 43, 1312-1317 (1951).
[32] Loparev, V.P., "Experimental investigation of the atomization of drops of liquid under conditions of a gradual rise of the external forces", *Izv. Akad. Nauk SSSR, Mekh. Zhidkosti Gaza* 3, 174-178 (1975).
[33] Aalburg, C. Faeth, G.M. and van Leer, B. (2002) "Deformation and drop properties of round drops subjected to shock wave disturbances", *AIAA Paper* 2002-0341 (2002); also *AIAA J*., submitted.

[34] Gel'fand, B.E, Gubin, S.A., and Kogarko, S.M., "Various forms of drop fractionation in shock waves and their special characteristics", *Inzh.-Fiz. Zh*. 27, 119-126 (1974).
[35] Simmons, H.C., "The correlation of drop-size distributions in fuel nozzle sprays", *J. Engr. for Power* 99, 309-319 (1977).
[36] Belz, M.H., *Statistical Methods in the Process Industries*, Wiley, 1973, p. 103.
[37] Chorin, A. J., "Numerical solution of the Navier-Stokes equations", *Math. Comp*. 22, 745-755 (1968).
[38] Harlow, F.H., and Welch, J.E., "Numerical calculation of time-dependent viscous incompressible flow of fluid with free surface", *Phys. Fluids*, 8, 2182-2189 (1965).
[39] Sussman, M., Smereka, P., and Osher, J., "A level set approach for computing solutions to incompressible two-phase flow", *J. Comp. Phys*. 114, 146-159 (1994).
[40] Sussman, M., and Fatemi, E., "An efficient, interface-preserving level set redistancing algorithm and its application to interfacial incompressible flow", *SIAM J. Sci. Comp*. 20, 1165-1191 (1999).
[41] Brackbill, J.U., Kothe, D.B., and Zemach, C., "A continuum method for modeling surface tension", *J. Comp. Phys*. 100, 335-354 (1991).
[42] Taneda, S., "Experimental investigation of the wake behind a sphere at low Reynolds numbers", *J. Phys. Soc. Japan* 11, 1104-1108 (1956) .
[43] Roos, F.W., and Willmarth, W.W., "Some experimental results on sphere and disk drag", *AIAA J*. 9, 285-291 (1971).